International Journal of Heat and Fluid Flow 115 (2025) 109848

Contents lists available at ScienceDirect

International Journal of Heat and Fluid Flow

journal homepage: www.elsevier.com/locate/ijhff

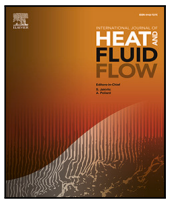

Predicting the global drag of turbulent channel flow over roughness strips

Jonathan Neuhauser *, Carola Schmidt, Davide Gatti, Bettina Frohnapfel

Institute of Fluid Mechanics, Karlsruhe Institute of Technology, Kaiserstr. 12, Karlsruhe, 76131, Germany

ARTICLE INFO

Keywords:
Heterogeneous roughness
Turbulent wall-bounded flows
Heat transfer
Global drag

ABSTRACT

Predicting the global drag of heterogeneous rough surfaces remains one of the great challenges in roughness research (Chung et al., 2021). In the limit where patch sizes are much larger than the boundary layer thickness, predictive formulas can be derived under the assumption that the flow is in local equilibrium with the surface properties (Neuhauser et al., 2022, Hutchins et al., 2023). The present work extends this concept to predict the drag behavior of turbulent channel flows over surfaces with spanwise heterogeneous roughness properties which vary over length scales comparable to the boundary layer thickness. The drag predictions are compared with high-fidelity measurements obtained in an air channel flow facility (Frohnapfel et al., 2024). As an outlook to future work, it is discussed how heat transfer over rough surface strips can be modeled under the local equilibrium assumption.

1. Motivation and approach

Drag predictions for flows over rough surfaces rely on the prescription of a homogeneous roughness length scale; i.e. an equivalent sandgrain roughness k_s. This quantity can be obtained empirically from drag measurements (physical experiments or numerical experiments based on DNS), through existing correlations with statistical surface properties (Chung et al., 2021) or recently also based on data-driven approaches (Lee et al., 2021; Yang et al., 2023). All approaches rely on reference data in form of Nikuradse-type curves, i.e. a friction coefficient (e.g. C_f) as a function of Reynolds number.

For rough surfaces whose roughness properties vary in space, there is no common understanding of how to predict the resulting global drag and reference data is rare. Recently, the local equilibrium assumption was used to arrive at predictions of global drag. It assumes that over each surface patch the flow behaves as if it was in equilibrium with the underlying surface condition. Corresponding global drag predictions were derived e.g. by Neuhauser et al. (2022) for turbulent channel flow and by Hutchins et al. (2023) for turbulent boundary layers. Both works consider roughness surface properties that are piecewise constant in the spanwise direction and independent of the streamwise direction and formulate expectations for the resulting global drag. These formulations differ between channel and boundary layer flows because of different underlying assumptions. Experimental reference data for both flow configurations are required to test the proposed drag prediction.

In the present work, we consider the turbulent channel flow with streamwise oriented roughness strips (i.e. finite spanwise extension of the individual surface patches but quasi infinite extension in streamwise direction) for which we have high-quality reference data available (Frohnapfel et al., 2024). The surfaces considered consist of streamwise aligned roughness strips (P60 sandpaper) which alternate with smooth surface parts of the same width. The width in terms of the channel half-height h is set to $s \approx h$ and $s \approx 2h$. The data set contains $C_f(Re_b)$ for these strip-type rough surfaces and for the homogeneous rough and smooth reference cases over a Reynolds number range $4500 < Re_b < 85\,000$ (where $Re_b = u_b 2h/\nu$ with bulk velocity u_b and kinematic viscosity ν).

The results shown in Fig. 1 were previously published in Frohnapfel et al. (2024). The alternating rough and smooth surface parts are arranged such that they have the same mean height, which corresponds to the case of submerged rough strips in this previous publication. In this case, the (average) channel height is identical for rough and smooth sections of the surface. As can be seen in Fig. 1, the drag curves for two different strip widths differ, despite the fact that 50% of the surface are rough in both cases. In addition, the data do not indicate fully rough behavior (i.e. a Re-independent C_f) for the rough strips within the Reynolds number range considered. However, there is an intermediate Reynolds number range in which the data appear to remain at a constant C_f similar to a fully rough behavior before dropping again to lower values. The question at hand is whether the observed $C_f(Re_b)$-relation for rough strips can be predicted based on $C_f(Re_b)$ for the homogeneous rough and homogeneous smooth surfaces alone.

* Corresponding author.
E-mail address: jonathan.neuhauser@kit.edu (J. Neuhauser).

https://doi.org/10.1016/j.ijheatfluidflow.2025.109848
Received 14 January 2025; Received in revised form 24 March 2025; Accepted 7 April 2025
Available online 18 April 2025

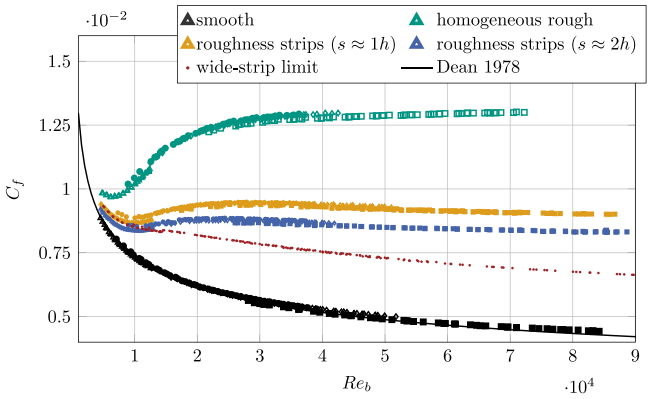

Fig. 1. Measurement data from Frohnapfel et al. (2024) (thick symbols for smooth and rough references and roughness strips with two different s) and wide-strip limit (Neuhauser et al., 2022). Different symbols within each color correspond to different flow rate measurement procedures within the experiment which is not in focus here. The roughness strips are symmetrically placed on channel top and bottom wall and are inserted in such a way that the average channel height in the rough channel parts is identical to the one in the smooth channel parts. The evaluation of the plotted C_f is based on this average channel height. (For interpretation of the references to color in this figure legend, the reader is referred to the web version of this article.)

Based on an equilibrium assumption (the flow is in local equilibrium with the boundary condition above each surface patch) an averaging procedure can be derived in which the global drag of the heterogeneous surface is predicted based on the drag behavior of the homogeneous reference surfaces. The resulting predictive curves for global drag are expected to be valid only for heterogeneous surfaces consisting of surface patches whose size significantly exceeds the boundary layer thickness. For the present case of streamwise aligned rough strips (spanwise heterogeneous roughness) we refer to the global drag prediction based on the equilibrium assumption as wide-strip limit. The wide-strip limit for a turbulent channel flow according to Neuhauser et al. (2022) is included in Fig. 1. It can be seen that it clearly underpredicts the measured C_f-curves indicating that the assumption of local equilibrium is indeed not valid. In fact, the wide-strip limit underestimates the drag for both s and most Reynolds numbers. While both cases have a 50% surface coverage their global drag differs, indicating that both surfaces induce different deviations from the wide-strip limit and the underlying equilibrium assumption.

The present contribution aims at improving this predictive quality by complementing the model with information about the finite width of the strips.

2. The original predictive model: the wide-strip limit

In a first step, we briefly review the prediction of the wide-strip limit which forms the starting point for the prediction of global drag on roughness strips. In the following, we refer to the global skin friction coefficient $\overline{C_f}$ in case of a heterogeneous rough surface and the related quantities with an overbar, whereas global quantities for homogeneous surfaces are written without overbar.

For a turbulent channel flow the streamwise pressure gradient at different spanwise positions has to be identical to allow for fully-developed flow conditions. Hence, the wide-strip limit for spanwise alternating smooth and rough strips is derived based on the idea that this identical pressure gradient will induce different flow rates depending on whether the surface is rough or smooth.[1]

The pressure drop - flow rate relation for each type of surface is obtained from the available $C_f(Re_b)$-relation for the homogeneous smooth and rough surface. These are valid for the subsurfaces of the heterogeneous surface if the assumption of local equilibrium holds. Fig. 2 depicts the idea of how an average of the homogeneously smooth and rough $Re_b - C_f$-curves (i.e. the wide-strip limit) is constructed based on the assumption of the same friction Reynolds number Re_τ, which is the consequence of assuming equal streamwise pressure gradient if the channel height of both sections is the same.

Since the channel half-height h of the smooth and the rough surface parts of the considered strip-type surfaces is the same, a constant mean streamwise pressure gradient $\Pi(= -\partial p/\partial x)$ corresponds to a constant friction Reynolds number Re_τ along both surface parts, as this is defined as

$$Re_\tau = \frac{u_\tau h}{\nu} = \sqrt{\frac{\tau_w}{\rho}}\frac{h}{\nu} = \sqrt{\frac{\Pi h}{\rho}}\frac{h}{\nu} \tag{1}$$

with the fluid's density ρ and kinematic viscosity ν.

The friction Reynolds number is not included in the classical $Re_b - C_f$ visualization. Therefore, the definition of the friction coefficient is reshaped such that it includes the bulk Reynolds number Re_b and the friction Reynolds number Re_τ

$$C_f = \frac{\tau_w}{\frac{\rho}{2}u_b^2} = 8\frac{Re_\tau^2}{Re_b^2}. \tag{2}$$

This relation is plotted for several constant values of Re_τ in Fig. 2. Whilst the friction Reynolds number is the same for both subsurfaces, the volume flow rate and thus the local bulk Reynolds numbers differ. Using the plotted relation, the local bulk Reynolds numbers are determined at the intersection points with the homogeneous curves. Volume-weighted averaging of the two values yields the global bulk Reynolds number in the channel. As the surfaces of interest are covered by 50 % with roughness, the global volume flow rate and thus the global bulk Reynolds number is obtained by taking the mean between the two local Reynolds numbers (if the roughness surface coverage was 30%, the effective Reynolds number would be calculated by $Re_{\text{eff}} = 0.3Re_{\text{rgh}} + 0.7Re_{\text{smooth}}$). The dedicated global friction coefficient still has to fulfill Eq. (2) and thus is the value on the plotted curve. Repeating this procedure for all friction Reynolds numbers results in the wide-strip limit which is drawn in magenta in Fig. 2.

Summarizing this averaging procedure mathematically results in a predicted friction coefficient based on a power mean as suggested by (Neuhauser et al., 2022)

$$\overline{C_f} = \left(\frac{1}{2}\left(\frac{1}{\sqrt{C_{f,\text{rgh}}}} + \frac{1}{\sqrt{C_{f,\text{smooth}}}}\right)\right)^{-2} \tag{3}$$

where $C_{f,\text{rgh}}$ and $C_{f,\text{smooth}}$ are taken at the same Re_τ.[2]

As discussed before, the present contribution aims to complement this modeling approach with information about the finite strip width. The extended modeling approach is based on the idea of a hydraulic channel height which is introduced in the following.

3. An additional model parameter: the hydraulic channel height of a rough-wall channel

Similar to a hydraulic diameter for duct flows, the hydraulic channel height refers to an effective channel height of a non-smooth channel

[1] A streamwise heterogeneous rough surface consisting of spanwise aligned roughness strips will feature identical flow rates in the rough and smooth surface sections (due to continuity) with varying pressure gradient. Therefore, the present prediction for $\overline{C_f}$ is not meaningful in this context.

[2] This is valid as long as smooth and rough channel parts have the same channel half-height. As will be discussed later, different channel height definitions are possible. For Eq. (3) to be (strictly) valid, the channel height chosen for data evaluation is the one that needs to be identical in both sections of the channel. Otherwise, a different formulation for $\overline{C_f}$ is required; see Frohnapfel et al. (2024).

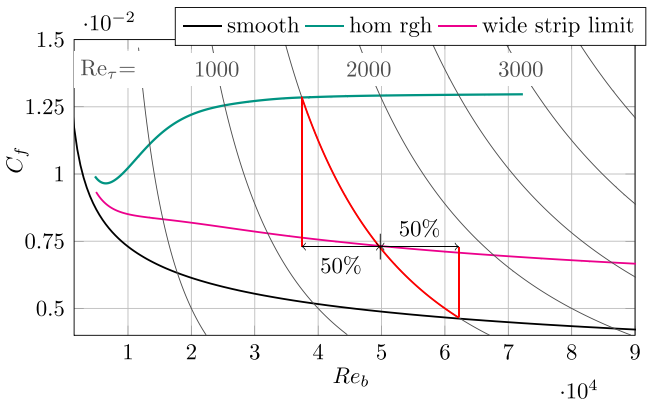

Fig. 2. Friction coefficient versus Re_b for the wide-strip limit at 50% roughness surface coverage which is based on input from the homogeneous smooth and rough reference curves only. The global $\overline{C_f}$ for the wide-strip limit is obtained based on $C_{f,\mathrm{rgh}}$ and $C_{f,\mathrm{smooth}}$ at the same Re_τ. The gray lines in the background are lines of constant Re_τ.

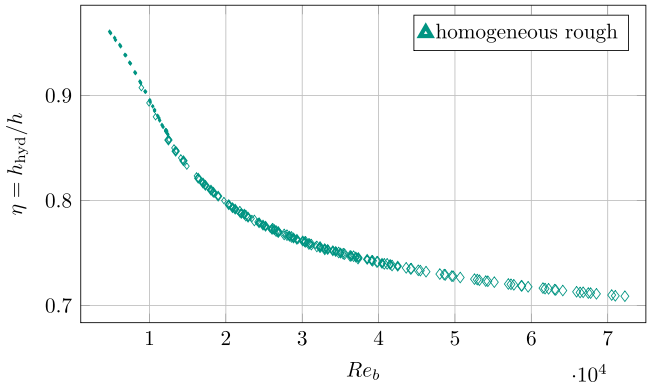

Fig. 3. Hydraulic channel height ratio $\eta = h_{\mathrm{hyd}}/h$ for P60 sandpaper.
Source: Data from Frohnapfel et al. (2024).

that recovers the $C_f(Re_b)$-relation for a smooth wall channel. In contrast to the hydraulic diameter for ducts, the hydraulic channel height is not defined based on geometric properties, but is derived as a result from a pressure drop and volume flow rate measurement (von Deyn et al., 2022; Frohnapfel et al., 2024). A rough-walled channel reduces the flow rate at a given pressure gradient Π compared to a smooth channel with the same (average) channel height. The hydraulic channel height corresponds to the reduced height of a smooth wall channel in which the flow rate measured for the rough wall channel is found for the same Π. Consequently, the hydraulic channel height is not only a function of the roughness (e.g. in terms of the equivalent sand grain size k_s) but also of the operating condition (in terms of Re_b or Π). The hydraulic channel half-height h_{hyd} normalized by the geometrical channel half-height h is shown in Fig. 3 for the homogeneous rough surface (P60 sandpaper). It can be seen that P60 sandpaper (placed homogeneously on both channel walls in our channel flow facility) induces a reduction of h_{hyd}/h by approx. 10% (almost 30%) at $\mathrm{Re_b} = 1\times10^4$ (7×10^4).

This observation is used to construct a modeling approach for the global friction coefficient of surfaces with streamwise aligned roughness strips. We assume that the combination of rough and smooth strips in a channel can be represented by a local narrowing of the channel. The idea is sketched in Fig. 4. The rough wall section of the channel is modeled as a channel with reduced height in such a way that a streamwise aligned ridge is inserted instead of the rough strip. We thus obtain a channel with streamwise aligned ridges in which the ridge height depends on the operating conditions, i.e. the applied pressure drop, in the channel. The width of the ridges corresponds to the width of the rough strips. Accordingly, the wide-strip limit is modeled by two neighboring (very wide) channels with different height. The same pressure gradient is applied to each of these channels, resulting in different flow rates: the channel with smaller channel height yields less flow-rate for the same pressure gradient.

In the following, the global flow behavior in the structured channel with ridges compared to its theoretical limit for very wide ridges is considered under laminar and turbulent conditions. Eventually, it is shown that the easy-to-obtain laminar results for the structured channel can be used to derive a correction for the wide-strip limit.

4. Deriving model-corrections: the global drag over streamwise-aligned ridges

We aim to estimate the global skin friction coefficient $\overline{C_f} = 2\overline{u_\tau}^2/\overline{u_b}^2$ (where $\overline{(\cdot)}$ denotes spanwise averaged quantities), expressed in terms of friction velocity u_τ and bulk velocity u_b, for a channel with structured walls. The global friction coefficient can also be expressed in terms of the mean pressure gradient Π,

$$\overline{C_f} = \frac{2\Pi\tilde{h}}{\rho\overline{u_b}^2} = \frac{8\Pi\tilde{h}^3}{\rho\overline{\dot{V}}^2} \tag{4}$$

where ρ is the fluid density $\tilde{h}$ is a reference channel half-height, to be defined later and $\overline{\dot{V}}$ is the spanwise averaged flow rate per unit width. As discussed before, we postulate that two flows which are both in local equilibrium with their respective boundary condition need to have the same mean streamwise pressure gradient in order to co-exist without a separating wall.

4.1. Laminar flow

For a laminar channel with spanwise alternating channel half-heights h_1 and $h_2 < h_1$ (see Fig. 5), in the limit of $s/h_i \gg 1$ (i.e. the additional surface area of the step and interface transients are negligible), the resulting skin friction coefficient may be computed analytically using the classical Hagen–Poiseuille relation:

$$\overline{C_f} = \frac{12}{\overline{Re_b}} \cdot \frac{\tilde{h}^3}{\frac{1}{2}(h_1^3 + h_2^3)} \quad \text{with} \quad \overline{Re_b} = \frac{\overline{u_b}2\tilde{h}}{\nu} \tag{5}$$

where $\tilde{h}$ is any reference height (to be defined). Note that $\overline{u_b}$ is the volumetric flow rate per unit width divided by $\tilde{h}$. Therefore, $\overline{Re_b}$ is independent of the choice of $\tilde{h}$ for a known flow rate.

The choice of the reference height $\tilde{h}$ is relevant when comparing the skin friction coefficient of different setups, and poorly understanding the influence of the reference height may prompt problematic statements regarding changes in drag. Therefore, we consider different choices for $\tilde{h}$ in the evaluation of $\overline{C_f}$. The corresponding results are shown in Fig. 6. All plots show the numerically evaluated $\overline{C_f Re_b}$ for different ridge dimensions. The ridge geometry is characterized by its height $\Delta h = h_2 - h_1$ and its width s/h_1.

Three different choices for the reference channel half-height are considered. The first is the 'empty channel height' $\tilde{h} = h_{empty} = h_1$ (Fig. 6(a)) and the second is a 'meltdown height' $\tilde{h} = h_{avg} = 1/2(h_1+h_2)$ (Fig. 6(b)). The dashed red line in these plots corresponds to the analytical solution of a smooth wall laminar channel flow $\overline{C_f Re_b} = 12$ and the blue dashed line represents the limit for very wide ridges ($s/h_i \gg 1$) according to Eq. (5). The obtained results in these two plots can easily lead to different conclusions for one and the same numerical results.

Using $\tilde{h} = h_{empty}$ (Fig. 6(a)) yields an increase in $\overline{C_f}$ with increasing ridge height $\Delta h = h_2 - h_1$, while using $\tilde{h} = h_{avg}$ (Fig. 6(b)) yields a decrease in $\overline{C_f}$ with increasing ridge height (for the limiting case of $h_2 \to 0$, a 'skin friction reduction' of 75% can be observed).[3] A third

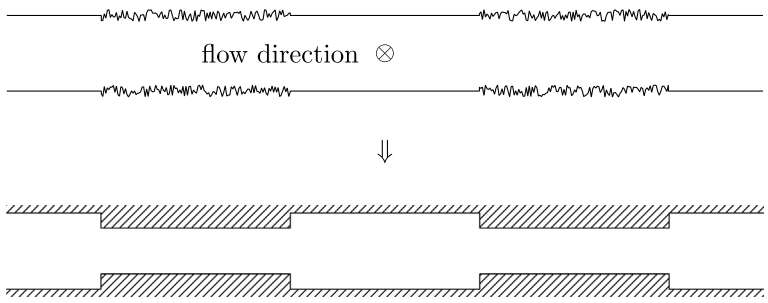

Fig. 4. Sketch of the modeling approach: Rough strips are identified with a locally narrower channel.

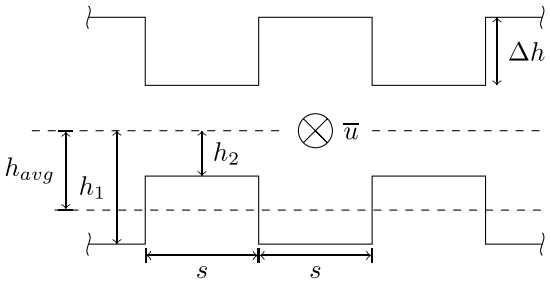

Fig. 5. Sketch of the spanwise periodic ridge-type setup. Mean flow direction is perpendicular to the drawing plane.

alternative is shown in Fig. 6(c). It is introduced to recover the smooth wall solution $\overline{C_f}\,\overline{Re_b} = 12$ for very wide ridges. Here, the reference channel half-height is defined as:

$$\tilde{h} = h_{lam} = \sqrt[3]{\frac{1}{2}\left(h_1^3 + h_2^3\right)}, \tag{6}$$

h_{lam} is the half-height of the (homogeneous smooth-wall) channel that has the same relationship between $\dot{V}$ and Π as the channel with ridge heights h_1 and h_2, for $s/h_i \gg 1$.

As anticipated $\overline{C_f}$ is independent of the ridge height in the limit of large s when evaluated based on h_{lam} (Fig. 6(c)) and $\overline{C_f} = 12/\overline{Re_b}$ is recovered in this case. The visible deviation from $\overline{Re_b} \cdot \overline{C_f} = 12$ for smaller strip sizes s/h_1 and large ridge heights $\Delta h/h_1$ stems from the fact that the flow is not in local equilibrium. This plot thus provides a measure for the impact of the transition region between the two flow regions on the global drag.

In addition, we observe that for a given pressure gradient, the flow rate per unit width $\dot{V}$ tends towards the equilibrium condition in the thinner part of the channel, but not equally so in the thicker part of the channel (since $h_1 > h_2 \rightarrow s/h_1 < s/h_2$) where it remains below the equilibrium condition. In consequence, for finite ridge widths, the global flow rate for a given pressure gradient is lower than in case of very wide ridges.

4.2. Turbulent flow

In the following, we compare these results to the case of turbulent flow over ridges. Similar to the laminar case, an explicit expression for the global friction coefficient for the case of $s \gg h_i$ can be given based on the correlation of Dean (1978), $C_f = 0.073 Re_b^{-1/4}$. We find

$$\overline{C_f} = 0.073\,\overline{Re_b}^{-1/4} \frac{\tilde{h}^3}{\left(\frac{1}{2}\left(h_1^{12/7} + h_2^{12/7}\right)\right)^{7/4}}. \tag{7}$$

In analogy to the laminar case it is possible to define a channel half-height that recovers the smooth wall correlation (which is given by the Dean correlation $\overline{C_f}\,\overline{Re_b}^{1/4}/0.073 = 1$ for turbulent flow) for very wide ridges:

$$\tilde{h} = h_{turb} = \left(\frac{1}{2}\left(h_1^{12/7} + h_2^{12/7}\right)\right)^{7/12}. \tag{8}$$

In order to investigate the influence of finite s under turbulent flow conditions, DNS simulations of channel flow with streamwise aligned ridges have been performed for the cases listed in Table 1. The employed numerical code is NekRS, a portable version of the spectral element code Nek5000 (Fischer et al., 2022). The simulations were set-up using a body-conform mesh and streamwise periodicity, with streamwise box length $L_x = 4\pi h_1$. Element order $n = 7$ and BDF3/EXT3 timestepping was used. The simulations were conducted at a prescribed constant global flow rate.

Table 1
Metadata for discussed turbulent cases.

s/h_1	$\Delta h/h_1$	L_z/h_1	N_{el}	Re_b
–	0	4	153 600	8000
1	0.132	4	475 200	12 000
1	0.25	4	124 800	8000
1	0.5	4	110 400	8000
2	0.25	4	124 800	8000
2	0.5	4	123 200	8000
8	0.25	16	499 200	8000
8	0.5	16	492 800	8000

Fig. 7 shows the resulting skin friction coefficients for different choices of $\tilde{h}$ in analogy to the laminar results shown in Fig. 6. The smooth wall reference $\overline{C_f}\,\overline{Re_b}^{1/4}/0.073 = 1$ is indicated by a black line in these plots. The colored horizontal lines (orange, green, blue) on the right ordinate of each plot depict the limiting case of very wide ridges for the three considered values of Δh. For increasing s, the computed values for $\overline{C_f}$ clearly decrease towards the respective limiting cases, which collapse onto the smooth wall reference when using h_{turb}. Similar to the laminar results discussed before, a 'skin friction drag reduction' can be obtained for high s, when evaluating the numerical data using h_{avg}. We note that there is no right or wrong choice for $\tilde{h}$ in the evaluation of C_f. The different choices simply lead to a presentation of the results that are likely to be interpreted differently. For any data evaluation of this type it is thus of utmost importance to communicate how an evaluation of $\overline{C_f}$ was performed.

For the present study it is important to realize that there is a qualitative similarity between laminar (Fig. 6) and turbulent (Fig. 7) cases, irrespective of the choice of $\tilde{h}$, which suggests that the effect of finite s on $\overline{C_f}$ is mostly a geometric one. This is also supported by closer

[3] This statement generally also holds for walls that are not shaped like a step function, e.g. Daschiel et al. (2012) reported a 50% 'drag reduction' for a channel with sinusoidal walls at the limit of large wavelengths, where the skin friction is evaluated with h_{avg}.

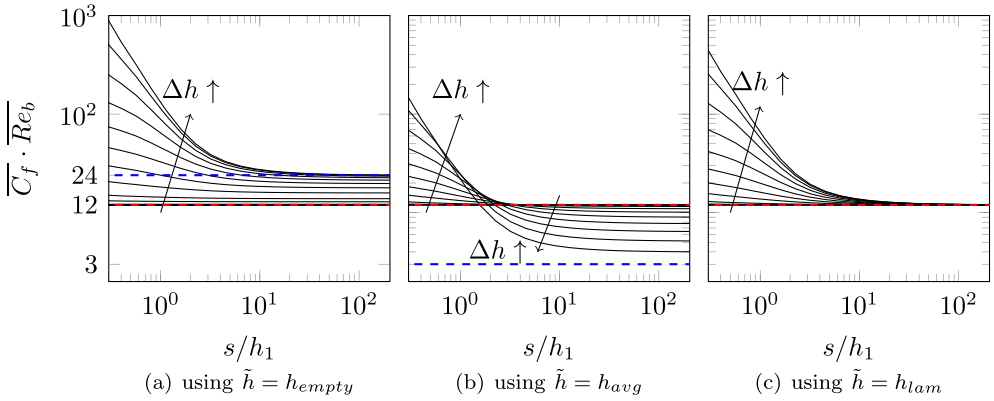

Fig. 6. Product of $\overline{Re_b}$ and $\overline{C_f}$ for laminar flow over streamwise-aligned ridges. Displayed are $\Delta h/h_1 = 0.1, 0.2, \ldots, 0.9$, (dashed red) the value from the canonical laminar relation, $\overline{Re_b} \cdot \overline{C_f} = 12$ and (dashed blue) the $s \to \infty$ asymptote for the case $h_2 \to 0$. (For interpretation of the references to color in this figure legend, the reader is referred to the web version of this article.)

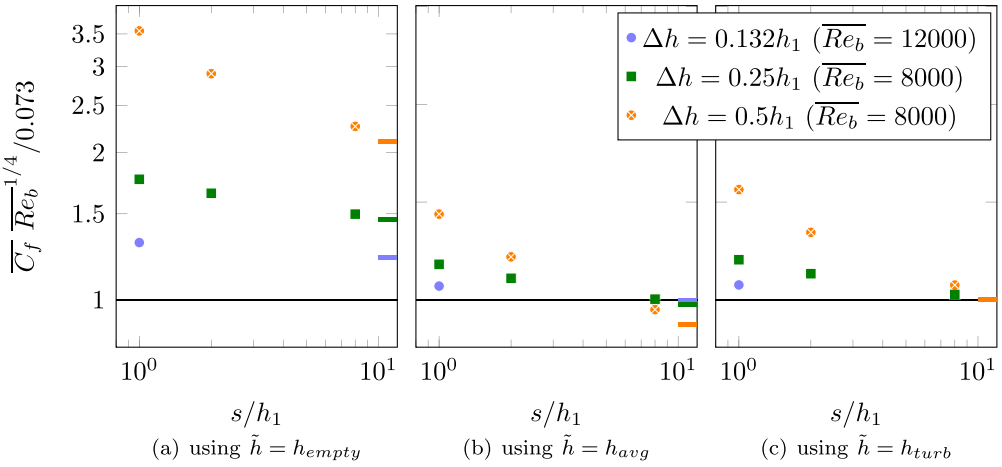

Fig. 7. Diagnostic function $\overline{C_f}\ \overline{Re_b}^{1/4}/0.073$ for the considered turbulent cases. Displayed are $\Delta h/h_1 = 0.25$ (green), 0.5 (orange) and 0.132 at a higher Reynolds number. The colored horizontal lines on the right-hand axis of each subplot indicate the expected value for very large s, i.e. the wide-strip limit. The subplots are evaluated with different definitions for $\tilde{h}$. Due to the definition of h_{turb}, the wide-strip limit is equal to 1 for all cases in subplot (c). (For interpretation of the references to color in this figure legend, the reader is referred to the web version of this article.)

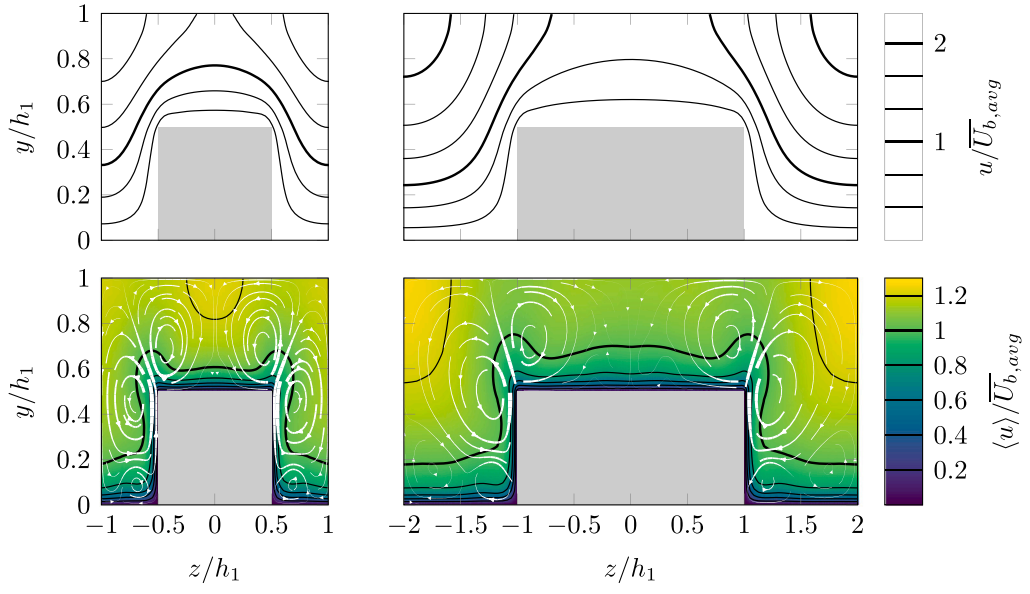

Fig. 8. Comparison of laminar (top) and turbulent (bottom) flow over streamwise-aligned ridges for $\Delta h = 0.5h_1$. Left: $s/h_1 = 1$, Right: $s/h_1 = 2$. Top: Laminar flow at constant bulk flow rate, Bottom: Turbulent flow at constant bulk flow rate ($\overline{Re_b} = 8000$). The resulting secondary flow is indicated with streamlines, line thickness of the streamlines indicates magnitude; maximum magnitude is $5.3\%\overline{U}_{b,avg}$ ($s/h_1 = 1$) and $5.5\%\overline{U}_{b,avg}$ ($s/h_1 = 2$). (For interpretation of the references to color in this figure legend, the reader is referred to the web version of this article.)

investigation of the spanwise distribution of streamwise velocity as discussed in the following. Fig. 8 depicts contours of streamwise velocity in part of the channel cross section for the laminar (top) and turbulent (bottom) case for two different ridge widths. We recall that the width of the ridge and of the valley between the ridges is always identical in the present study since the ridges resemble surface roughness that covers 50% of the surface. The velocity contours in the turbulent flow case are significantly more complex than the laminar one since turbulent secondary flow develops in the presence of ridges. This mean flow in the spanwise and wall-normal velocity component is indicated by the white in-plane streamlines Fig. 8 (bottom) which are placed in front of a color map of the streamwise mean velocity. The turbulent secondary flow clearly impacts the streamwise velocity distribution. Nevertheless, the laminar and turbulent contours of streamwise velocity carry some similarities when one considers the changes that occur with increasing ridge width.

Consider the wall-normal gradient of the streamwise mean velocity (i.e. the local wall shear stress) for $s/h_1 = 1$ (left) and $s/h_1 = 2$ (right). For each flow condition, laminar and turbulent, the wall shear stress distribution on the ridge sides and the ridge top, close to the edge remains very similar when doubling the ridge width. On top of the ridge the flow rate decreases with increasing s (less contours in the laminar case, lower values of $\overline{u}$ in the turbulent case) which also results in a reduction of the shear stress in the ridge center. With increasing s there is a flow rate increase above the valley for laminar and turbulent flow which is mostly located further away from the wall while the wall shear stress remains similar. This results in a smaller total wall shear stress for the wider ridge as reflected by the decrease in the diagnostic function ($\overline{Re_b C_f}$ for the laminar case, $\overline{Re_b}^{1/4}\overline{C_f}$ for the turbulent case) with increasing s for laminar and turbulent flow conditions.

The observed increase in the diagnostic function with smaller s can be translated into a 'flow rate loss'. In the limiting case of very wide ridges (and valleys) the maximum achievable global flow rate for a given pressure gradient is realized. The finite width of ridges (and valleys) reflects in a reduction of the achievable flow rate compared to the expected maximum one. The relative flow rate loss is thus defined as

$$R_{\dot{V}} = 1 - \frac{\overline{\dot{V}_{actual}}}{\overline{\dot{V}_{expected,limit}}} \tag{9}$$

Table 2 shows the results for all considered laminar and turbulent cases. As expected $R_{\dot{V}}$ is positive, indicating that the achievable flow rate for ridges (and valleys) with finite width is lower than the expected one for very wide ridges. The data show that $R_{\dot{V}}$ increases with larger Δh and smaller s for both, laminar and turbulent flow conditions. To first approximation, the obtained values for $R_{\dot{V}}$ agree reasonably well for laminar and turbulent flow, which supports the hypothesis that the friction increase due to narrower ridges (i.e. the deviation from the equilibrium state) is mainly a geometric and not a turbulent effect, despite the emergence of strong secondary flow in the turbulent case. Stated differently, the deviation from the limiting equilibrium case is mainly caused by the transients between the subdomains, and those transients and their effect is comparable in magnitude for the laminar and turbulent regime. In addition, we note that $R_{\dot{V}}$ is independent of the prescribed pressure gradient (and thus the Reynolds number) in the laminar regime while a (small) Reynolds number dependency is expected for turbulent flow conditions.

Table 2
Relative flow rate loss $R_{\dot{V}} = 1 - \overline{\dot{V}_{actual}}/\overline{\dot{V}_{expected,limit}}$ for the pressure gradient encountered in the respective simulations in which Re_b was prescribed. Note that for the laminar case, $R_{\dot{V}}$ is independent of pressure gradient or Reynolds number.

s/h_1	$\Delta h/h_1$	$R_{\dot{V}}$ (turbulent)	$R_{\dot{V}}$ (laminar)
1	0.132	0.0393	0.0332
1	0.25	0.1024	0.1125
1	0.5	0.2568	0.3468
2	0.25	0.0679	0.0580
2	0.5	0.1661	0.1837
8	0.25	0.0141	0.0133
8	0.5	0.0390	0.0448

5. Formulation of a new predictive model

In the next step, we employ $R_{\dot{V}}$ as a correction factor to the existing global drag prediction for the wide-strip limit (see Eq. (3)). This correction factor leads to a surface-specific flow rate reduction for a prescribed pressure drop or - in other words - to an increase in $\overline{C_f}$ for a certain $\overline{Re_b}$. This general tendency is in agreement with our observations for Fig. 1: The measured values of $\overline{C_f}$ are higher than those predicted by the wide-strip limit and indicate a surface-specific global drag.

Based on the observed similarity in the relative flow rate loss for laminar and turbulent flows over streamwise aligned ridges, we decide to employ the laminar reference data to formulate a new predictive model for the global drag of spanwise heterogeneous rough surfaces.

The existing (wide-strip limit) model for the global drag prediction relies on the assumption of a local equilibrium of the flow with the surface condition and thus only requires the drag curves for the homogeneous references (homogeneous smooth and homogeneous rough (P60)) as model input. The resulting global $\overline{C_f}$ for 50% roughness coverage is computed from the arithmetic mean of flow rates for the homogeneous smooth and the homogeneous rough case at a given pressure gradient, which is identical to the power mean average for $\overline{C_f}$ in Eq. (3) where homogeneous reference values are taken at the same Re_τ. This model is expected to be valid for the limiting case of rough strips with large spanwise dimension. It is corrected for finite size width of the roughness strips based on the relative flow rate loss as described in the following.

We hypothesize that the friction behavior, in particular the spanwise transients before a local equilibrium with the wall boundary condition is reached, is similar to that found in a channel flow with streamwise-aligned ridges.[4] Due to the discussed similarity between turbulent and laminar data in respect to these transients we rely on the laminar data for the model formulation. While h_1 is defined by the geometrical channel half-height and s by the strip width, a definition for $\Delta h = h_1 - h_2$ remains to be chosen. This is done in the following way: The prediction of the global drag coefficient in the wide-strip limit relies on two contributions to the global flow rate: one in the smooth section of the channel $\dot{V}_{smooth}$ and one in the rough section of the channel $\dot{V}_{rough}$. The ratio of these two contributions $\dot{V}_{rough}/\dot{V}_{smooth}$ can be easily computed for any Reynolds number. Similar ratios are computed for the laminar flow in the structured channel with very wide ridges (and valleys). In this case, the global flow rate consists of the flow rate in the channel section with height h_1 ($\dot{V}_{h1}$) and the flow rate in the channel section with height h_2 ($\dot{V}_{h2}$). This yields a flow rate ratio $\dot{V}_{h2}/\dot{V}_{h1}$ for every $\Delta h = h_1 - h_2$. The remaining model parameter Δh is now chosen such that $\dot{V}_{rough}/\dot{V}_{smooth} = \dot{V}_{h2}/\dot{V}_{h1}$. Since $\dot{V}_{rough}/\dot{V}_{smooth}$ depends on the applied pressure gradient, Δh is not constant for one particular type of roughness, but depends on the operating condition Π.

Once h_1, s and Δh are fixed for each Π, the correction factor $R_{\dot{V}}$ is extracted for the corresponding laminar database of the structured channel. This correction factor is used to compute the actual flow rate that enters Eq. (4) following Eq. (9). The reduced global flow rate results in an increase of the predicted global friction coefficient which depends on the operating conditions and the strip width.

When comparing the prediction with the measurement data, attention must be paid to the choice of $\tilde{h}$, which appears directly in Eq. (4).

[4] This requires that the additional drag introduced by the ridge side walls does not dominate, as is the case for $s \to 0$.

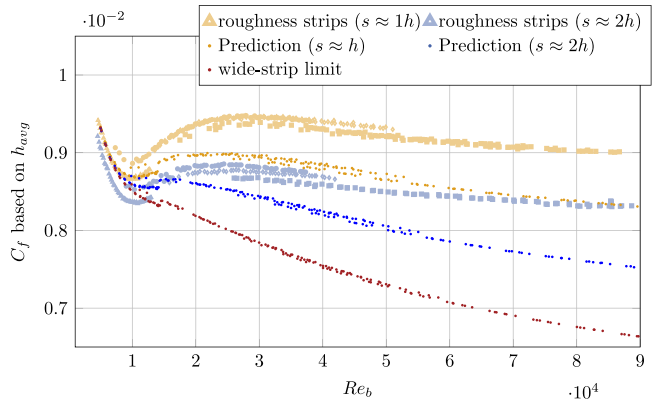

Fig. 9. Model predictions for the friction coefficient of rough strips of width $s \approx h$ and $s \approx 2h$ in comparison to the wide-strip limit and the measurement data of Frohnapfel et al. (2024). While light yellow and blue colors represent the measurement data for $s \approx h$ and $s \approx 2h$, respectively, the different symbols within each color correspond to different flow rate measurement procedures within the experiment. (For interpretation of the references to color in this figure legend, the reader is referred to the web version of this article.)

For the presented experimental results, the pressure drop and the volume flow rate in the channel flow facility was measured and translated into C_f and Re_b based on the geometrical (average) channel height (of the channel with the rough strips; i.e. h_1). The same choice needs to be taken in the model-based prediction to enable comparability. This issue is of minor concern for the present data set of submerged rough strips where the rough patches do not have a different mean height as the smooth ones. However, if the rough strips protruded significantly above the smooth ones, care should to be taken that the experimental data evaluation and the model prediction rely on the same channel height definition.

6. Results of the new predictive model

Fig. 9 shows the obtained predictions for $\overline{C_f}$ for two different values of s along with the experimental data. Results for the narrower strips $s \approx h$ are displayed in yellow and for the wider strips $s \approx 2h$ in blue. It can clearly be seen that the agreement with experimental data is significantly improved compared to the wide-strip limit (in brown). We note that the scatter in the experimental data is mainly related to uncertainties in the volume flow rate measurement; details can be found in the appendix of Gatti et al. (2015). Therefore, different symbols are used to distinguish data points with different flow rate measurements (in the sense that the orifice plates of an orifice flow meter were changed).

The new prediction correctly captures the measured effect of larger $\overline{C_f}$ for smaller s. In fact, the obtained agreement between prediction and measurements is surprising considering the strong simplifications introduced in the model formulation. Therefore, the quantitative agreement might be coincidental to some degree. In our opinion, the observed qualitative agreement of the predicted drag behavior is the most important result. The predictive model captures different regimes of the $\overline{C_f}(\overline{Re_b})$-curve. This includes effects at low Re_b (small difference between different values for s since homogeneous flow rates also differ less), intermediate Re (near-constant C_f over a limited Re range) and high Re_b (decreasing C_f).

Based on these model results, the emergence of an apparent fully rough condition in an intermediate Reynolds number range can be related to a strongly simplified interplay of the two subsurfaces, in which only a spanwise flow rate variation is considered. The model suggests that a range of constant $\overline{C_f}$ will be more pronounced for narrow surface structures and less pronounced for wider ones. The validity of this prediction remains to be verified by future measurements.

7. Extension to heat transfer

In this section, we will present preliminary results on whether the wide-strip limit (corrected by some geometry factor) can be generalized to estimate the heat transfer over inhomogeneous rough walls. Due to the lack of experimental reference data, we will not attempt to determine correction factors. However, we show that for the transport of a passive scalar inside a channel with streamwise homogeneity, a similar local equilibrium to Eq. (3) can be derived for the limit of large spanwise extension of the surface patches with homogeneous properties each. In such a setup, different boundary conditions for the temperature can be considered; we restrict ourselves to the case of what is commonly referred to as mixed boundary condition (Kasagi et al., 1992), i.e. the mean temperature increases linearly, but after subtraction of this linear increase, the wall temperature is zero everywhere, including vanishing fluctuations on the wall.[5]

For simplicity, we consider laminar flow here, but the analysis is possible in a similar fashion for fully-developed turbulent flow as well. The dimensional steady-state temperature equation for fully developed laminar flow in x direction is given by

$$\rho c_p u_x \frac{\partial T}{\partial x} = \lambda \left(\frac{\partial^2 T}{\partial y^2} + \frac{\partial^2 T}{\partial z^2} \right). \tag{10}$$

In particular, the streamwise gradient of temperature must be identical everywhere. Under fully-developed laminar conditions, the temperature profile for a channel with half-height h is given by Shah and London (1978) as

$$T(y) = T_w - \frac{3}{2}\frac{q}{h\lambda}\left(\frac{5}{12}h^2 - \frac{y^2}{2} + \frac{y^4}{12h^2} \right), \tag{11}$$

where q and T_w are heat flux density and wall temperature, respectively. A suitable Nusselt number definition is presented by Shah and London (1978) as

$$Nu = \frac{q D_h}{k(T_w - T_m)} = \frac{q D_h}{k}\left(T_w - \frac{\int_A T u_x \mathrm{d}A}{\int_A u_x \mathrm{d}A} \right)^{-1}, \tag{12}$$

with the classical hydraulic diameter $D_h = 4A/P$, four times the ratio of cross sectional area and perimeter of the profile. In the wide-strip limit, we expect the profile given by Eq. (11) to be obtained in a piecewise sense. The heat flux density q can be computed from a global energy balance: the total convective flux balances the total heat flux over the wall, and the streamwise temperature gradient is the same in both regions. The integrals in Eq. (12) are readily obtained from the assumed profile in both regions. We finally obtain the wide-strip limit of the Nusselt number for laminar flow as

$$\overline{Nu}_{s\to\infty} = \frac{140}{17}\frac{(h_1+h_2)(h_1^3+h_2^3)^2}{4(h_1^7+h_2^7)}. \tag{13}$$

The canonical value of $140/17 \approx 8.235$ (Shah and London, 1978) for the flat-plate channel is recovered for $h_1 = h_2$.

Fig. 10a displays the Nusselt number as defined by Eq. (12) obtained from laminar, body-fitted OpenFOAM simulations, as a function of strip size s and the height ratio $\Delta h/h_1 = (h_2 - h_1)/h_1$. Fig. 10b displays the Nusselt number normalized with the wide-strip limit for each Δh according to Eq. (13). While the full picture is more complex than for the streamwise momentum (see Fig. 6), we observe that for all height ratios, the wide-strip limit correctly captures the behavior for large s, and the deviation from the wide-strip limit generally increases with $\Delta h/h_1$.

[5] For constant heat flux, we observe that even in case of very wide strip, a temperature gradient in spanwise direction remains present over each section; hence the last term in Eq. (10) is expected to be non-negligible even for very wide strips. While a wide-strip limit may exist in this case, it cannot be derived from the local equilibrium assumption.

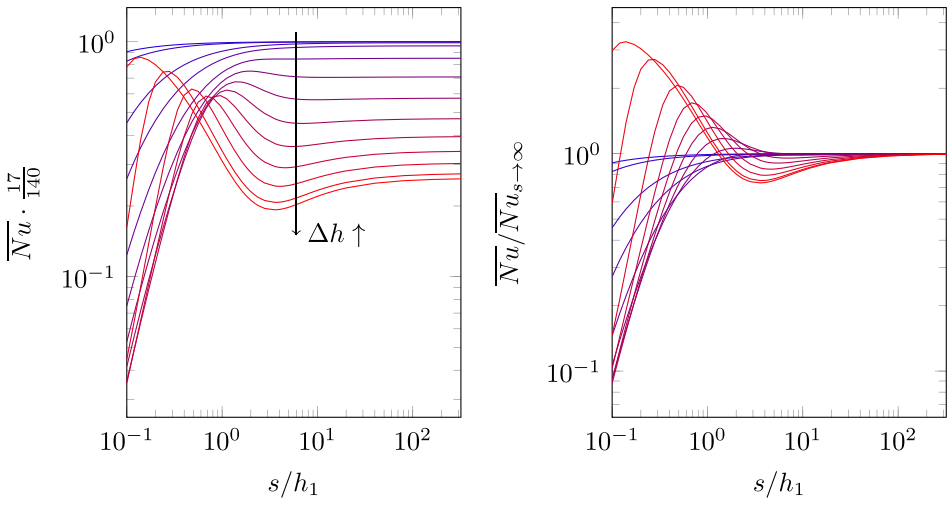

Fig. 10. Nusselt number normalized with the value of the flat-plate channel (a) as well as Nusselt number normalized with the wide-strip limit (b), see Eq. (13), for laminar flow over streamwise-aligned ridges. Displayed are $\Delta h/h_1 = 0.001, 0.005, 0.01, 0.05, 0.1, 0.2, \ldots, 0.9, 0.095$, ranging from blue to red. (For interpretation of the references to color in this figure legend, the reader is referred to the web version of this article.)

8. Summary and discussion

In this paper, we present a framework for predicting a global friction coefficient for turbulent channel flows over spanwise heterogeneous surfaces. The surface of interest is composed of spanwise alternating smooth and rough strips in which the roughness does not protrude but is arranged in such a way that its mean height is equivalent to the location of the smooth wall.

For the limit of a surface structure with large strip width, a prediction of the global $\overline{C_f}$ for the heterogeneous surface can be obtained from the $C_f(Re_b)$ behavior of the comprising surfaces (Neuhauser et al., 2022). The underlying assumption is that the flow above each strip is in equilibrium with its boundary conditions. For roughness strips with a width in the order of the boundary layer thickness such a prediction fails. The measured global friction coefficient significantly exceeds its predicted value, in particular at high Reynolds number where the difference between C_f of the smooth and the rough surface is large. A clear prediction improvement can be obtained when the transients between the equilibrium conditions are included in the model formulation. A simple model for the impact of these transients is obtained by exploiting the drag behavior of laminar channel flow with streamwise aligned ridges. The analogy of a roughness strip with a protruding ridge is deduced from the observation that a rough wall effectively reduces the hydraulic channel height (Frohnapfel et al., 2024).

The resulting prediction of the global $\overline{C_f}$ for this heterogeneous surface is in very good agreement with measurement data, correctly capturing the measured difference in global drag for roughness strips of different width with identical roughness coverage (50% of the total surface). Most importantly, the qualitative trend of the global drag curve is captured by the model. This indicates that the observed global drag behavior over rough strips which reveals a surprising plateau of $\overline{C_f}$ in some Reynolds number range can be related to spanwise flow rate variations. The agreement obtained with experimental data suggests that the spanwise transients of local flow rates are of significant relevance in internal flows with spanwise heterogeneous rough surfaces. In fact, they appear to dominate the deviation from the local-equilibrium assumption for the present data set.

Finally, we note that the employed model is highly simplified. It ignores the impact of turbulent secondary motions which tend to induce larger flow rates in the channel section with rough surface patches (Hinze, 1973; Frohnapfel et al., 2024). In addition, the presented predictive model is limited to spanwise heterogeneous roughness patterns. Patchy rough surfaces with streamwise variations are not expected to follow the prediction of Eq. (3) even for very large patches when the equilibrium assumption is justified. Further work and further reference data is required to advance predictive models for patchy rough surfaces. In the context, the present results underline the relevance of flow rate variations within the surface region of interest. To which extent results from internal flows (channel flows in the present case) can be transferred to drag prediction of external flows (spatially developing turbulent boundary layers) remains to be investigated in future work.

As further outlook, we demonstrated that the approach of a wide-strip limit can be extended to heat transfer, and that the Nusselt number obtained in this way agrees well with laminar simulations. Further numerical and experimental data on heat transfer over spanwise-heterogeneous rough surfaces is required to assess whether the model presented herein can also be applied to heat transfer in turbulent channel flow over finite-sized streamwise-aligned roughness strips.

CRediT authorship contribution statement

Jonathan Neuhauser: Writing – review & editing, Writing – original draft, Visualization, Validation, Software, Investigation, Formal analysis, Data curation, Conceptualization. **Carola Schmidt:** Writing – review & editing, Visualization, Investigation, Data curation. **Davide Gatti:** Writing – review & editing, Supervision, Project administration, Funding acquisition. **Bettina Frohnapfel:** Writing – review & editing, Writing – original draft, Supervision, Project administration, Funding acquisition, Conceptualization.

Declaration of competing interest

The authors declare that they have no known competing financial interests or personal relationships that could have appeared to influence the work reported in this paper.

Acknowledgments

We greatly acknowledge the support by the German Research Foundation (DFG) under research projects 462658330 and 521110788 and by High Performance Computing Center Stuttgart (HLRS), project ct-bctpf.

Data availability

Data will be made available on request.

References

Chung, D., Hutchins, N., Schultz, M.P., Flack, K.A., 2021. Predicting the drag of rough surfaces. Annu. Rev. Fluid Mech. 53 (1), 439–471.

Daschiel, G., Baier, T., Saal, J., Frohnapfel, B., 2012. On the flow resistance of wide surface structures. PAMM 12 (1), 569–570.

Dean, R.B., 1978. Reynolds number dependence of skin friction and other bulk flow variables in two-dimensional rectangular duct flow. J. Fluids Eng. 100 (2), 215–223.

Fischer, P., Kerkemeier, S., Min, M., Lan, Y.-H., Phillips, M., Rathnayake, T., Merzari, E., Tomboulides, A., Karakus, A., Chalmers, N., Warburton, T., 2022. NekRS, a GPU-accelerated spectral element Navier–Stokes solver. Parallel Comput. 114, 102982.

Frohnapfel, B., von Deyn, L., Yang, J., Neuhauser, J., Stroh, A., Örlü, R., Gatti, D., 2024. Flow resistance over heterogeneous roughness made of spanwise-alternating sandpaper strips. J. Fluid Mech. 980.

Gatti, D., Güttler, A., Frohnapfel, B., Tropea, C., 2015. Experimental assessment of spanwise-oscillating dielectric electroactive surfaces for turbulent drag reduction in an air channel flow. Exp. Fluids 56 (5).

Hinze, J.O., 1973. Experimental investigation on secondary currents in the turbulent flow through a straight conduit. Appl. Sci. Res. 28 (1), 453–465.

Hutchins, N., Ganapathisubramani, B., Schultz, M., Pullin, D., 2023. Defining an equivalent homogeneous roughness length for turbulent boundary layers developing over patchy or heterogeneous surfaces. Ocean Eng. 271, 113454.

Kasagi, N., Tomita, Y., Kuroda, A., 1992. Direct numerical simulation of passive scalar field in a turbulent channel flow. J. Heat Transf. 114 (3), 598–606.

Lee, S., Yang, J., Forooghi, P., Stroh, A., Bagheri, S., 2021. Predicting drag on rough surfaces by transfer learning of empirical correlations. J. Fluid Mech. 933.

Neuhauser, J., Schäfer, K., Gatti, D., Frohnapfel, B., 2022. Simulation of turbulent flow over roughness strips. J. Fluid Mech. 945.

Shah, R.K., London, A.L., 1978. Laminar flow forced convection in ducts: A source book for compact heat exchanger analytical data. Advances in Heat Transfer : Supplement, Academic Press, New York, Number 1.

von Deyn, L., Gatti, D., Frohnapfel, B., 2022. From drag-reducing riblets to drag-increasing ridges. J. Fluid Mech. 951.

Yang, J., Stroh, A., Lee, S., Bagheri, S., Frohnapfel, B., Forooghi, P., 2023. Prediction of equivalent sand-grain size and identification of drag-relevant scales of roughness – a data-driven approach. J. Fluid Mech. 975.